

A survey of TiO λ 567 nm absorption in solar-type stars

Fatemeh Azizi¹[★] and Mohammad Taghi Mirtorabi²[†]

¹Department of Physics, Payame Noor University (PNU), P.O.BOX 19395-3697, Tehran, Iran

²Department of Physics, Alzahra University, P.O. BOX 1993893973, Tehran, Iran

Accepted XXX. Received YYY; in original form ZZZ

ABSTRACT

Molecular absorption bands are estimators of stellar activity and spot cycles on magnetically active stars. We have previously introduced a new color index that compare absorption strength of the titanium oxide (TiO) at 567 nm with nearby continuum. In this paper we implement this index to measure long-term activity variations and the statistical properties of the index in a sample of 302 solar-type stars from the HARPS planet search program. The results indicate a pattern of change in star's activity, covers a range of periods from 2 years up to 17 years.

Key words: Activity cycles – Stars: Solar-type – Stars: active – Spectroscopic: visual band.

1 INTRODUCTION

Solar-type stars are $F8V - K2V$ main-sequences with $B - V$ color index between $0.48 \leq B - V \leq 0.8$. They covers more than 10 percent of nearby stars. Their spectral manifestation in visual region are full of spectral lines including molecular absorption bands. Molecular absorption is a fair indicator of cool regions like spots on the surface of active stars (Wallace et al. 2000). They can be used as a proxy to stellar oscillations, granulation, magnetic activity, plage and activity cycles.

Activity in solar-type stars is relatively old subject in astrophysics which has been addressed by many authors (Wilson 1968, 1978; Saar et al. 1997; Santos et al. 2000; Diaz et al. 2007; Boisse et al. 2009; Cincunegui et al. 2007; Lovis et al. 2011; Gomes da Silva et al. 2011). In late 60's Wilson (1968, 1978) introduced an index, S , to measures the $CaII H\&K$ lines emission. Diaz et al. (2007) have found $NaI D1\&D2$ lines useful to investigate activity in atmosphere of late-type dwarf stars. He observed a series of $F6$ to $M5.5$ dwarfs and found that these two lines can be used as activity indicator in stars with high level of activity and exhibit the Balmer lines in emission. Gomes da Silva et al. (2011) have computed activity in a sample of late M stars using indicators which was defined based on variability in a series of absorption lines including $CaII$, NaI and H_{α} . They found significant level of correlation between $CaII$ and NaI absorption and confirm that $NaI D1\&D2$ lines can be used as an activity indicator in stars with low level of activity. While Gomes da Silva et al. (2011) asserted that index manipulating HeI variability is a poor indicator of stellar activi-

ity, Saar et al. (1997) claimed, they have found correlation between $HeI D3$ and $CaII H\&K$ variation.

Solar-type spectra are also covered with molecular absorption. These are wide absorption bands which widely spread on the infra-red part of the spectrum. Berdyugina et al. (2000) showed that many molecular bands including Titanium Oxide (TiO) are indicators of solar magnetic fields concentrated in sunspots. This sensitivity can also be implemented as an indicator of stellar activity. Most of the previous investigations on molecular absorption bands was focused on near-infrared and longer wavelengths in coolest red giants and dwarf stars. Technical advancements in sensitivity and resolution of spectrographs make it possible to detect wide band absorption features made by temperature sensitive molecules like TiO in visual regions.

The near-infrared spectrum of cool late-type giant and dwarf stars are covered by wide and pervasive TiO absorption bands. TiO can survive in stellar atmosphere with surface temperature cooler than 4000 K. In hotter atmospheres TiO absorption can be used as a proxy to detect cool features like star spot. Long-term observation of TiO absorption in stellar spectrum can reveal stellar activity cycle. The idea that TiO bands could be used to measure spot's characteristics was first stated by Ramsey & Nations (1980). They observed the active star V711 Tau (HR1099) near its photometric minimum and found TiO absorption in its spectrum. They claim that the TiO absorption observed in the photosphere of the K1 IV star must be produced in a cooler region like a spot. Further observations by Neff et al. (1995); O'Neal et al. (1996) revealed TiO bands in spectra of other active stars and let them to estimate the spot's area and temperature. O'Neal et al. (1998) have used absorption bands of titanium oxide to study dark and cool stellar spots on magnetically active stars.

[★] E-mail: f.azizi@pnu.ac.ir (F.A.)

[†] E-mail: torabi@alzahra.ac.ir (M.T.M.)

As an indicator of TiO absorption in near-infrared, Wing (1992) introduced a photometric system consist of three filters, which measure the $TiO(\gamma, 0, 0)$ R-branch band head at 719 nm. He used this system to determine near-infrared magnitudes, near-infrared color index and spectral type of a sample of cool giant stars. He also recalibrate the color temperature relation of M type sub classes with his TiO -index. By careful investigation on the continuum band passes in Wings system in high resolution spectra of cool stars, Azizi & Mirtorabi (2015) have found that a small shift on continuum band passes (filters B and C) to shorter wavelengths will make the continuum less contaminated with weak absorption of VO bands and yields a better correlation between the index and surface temperature of the calibration stars¹.

Mirtorabi et al. (2003) used Wing photometric system to study the correlation between chromospheric activity and TiO absorption strength in the variable star λ Andromeda. They found an estimated activity cycle of about 4–14 years and an anti correlation between average TiO absorption (representing coverage of spots) and average visual brightness; similar to what is observed in the Sun. They also found that TiO molecules can survive even when the star is brightest, which means that part of the active regions might be distributed evenly on the surface of the star with no observable manifestation on the visual light curve.

We previously introduced a new color index (B-index) to measure the TiO absorption band strength centered at 567 nm (Bidaran, Mirtorabi & Azizi 2016). In that paper we showed that there is a clear correlation between the B-index and surface temperature of cool M giants where cooler atmospheres exhibits higher B-index. The index can be implemented as temperature indicator up to 4200 K where the TiO molecule breaks down and absorption bands disappear from the spectrum. Solar-type stars are too hot to have TiO molecules in their atmosphere but like the Sun if stellar activity is in close connection with appearance of cool spots in surface of the star then an active solar type star can exhibit significant B-index in spite of its hot atmosphere. In this work we implement our visual B-index to search for stellar activity in a sample of solar-type stars. The sample has been observed by the High Accuracy Radial Velocity Planet search Spectrograph (HARPS) at European Southern Observatory (ESO). This sample was already searched for stellar activity identification based on $CaII\ H&K$ lines by Lovis et al. (2011).

2 THE VISUAL ABSORPTION OF TITANIUM OXIDE

The B-index implements two narrow band filters. The first filter (D) is designed to measure TiO absorption band centered at 567 nm with full width at half-maximum (FWHM) of 16 nm. The depth of this absorption band

¹ The Wing three color photometric system consists of three filters. Filter A (FWHM = 11 nm) at 719 nm appropriately set to measure the strongest absorption bands of TiO in near infrared. Filter B (FWHM = 11 nm) with central wavelength at 754 nm and filter C (FWHM = 42 nm) with central wavelength of 1024 nm both are located in continuum region.

Table 1. The B-index Visual Filters.

Filter	Region Measured	Central Wavelength (nm)	Bandpass FWHM (nm)
D	$TiO\lambda 567$ nm band	567	16
E	Continuum	610	10

is compared with the nearby continuum with the second filter (E) at 610 nm with FWHM equal to 10 nm (Bidaran, Mirtorabi & Azizi 2016). The continuum filter was appropriately chosen to be free from molecular absorption. The central wavelengths and bandpass at these filters are listed in Table 1. By the way, the B-index is defined as

$$B - \text{index} = -2.5 \log \frac{\int F_D(\lambda) S_D(\lambda) d\lambda}{\int F_E(\lambda) S_E(\lambda) d\lambda} \quad (1)$$

where $F_D(\lambda)$ and $F_E(\lambda)$ are the integrated spectral flux in wavelength λ and $S_D(\lambda)$ and $S_E(\lambda)$ are appropriate filter response function.

3 THE STARS SAMPLE

We used a sample of 302 stars in FGK spectral type from the HARPS high-precision planet search program (Mayor et al. 2003). This sample was already used by Lovis et al. (2011) to study magnetic activity cycles and its correlation with HARPS precise radial velocities in solar-type stars by using $CaII\ H&K$ activity index. They implement a volume limited selection of stars closer than 56 pc, brighter than $V = 9.5$ mag and with a rotational velocity $vsini \leq 2\ km.s^{-1}$ in the solar neighborhood. These stars are slowly rotating and non binary or multiple. Thus, this sample represents an old single, solar-type stars. All stars have been observed by the 3.6 m telescope at European Southern observatory in *La Silla* using the HARPS spectrograph ($R \approx 115,000$). The original sample used by Lovis had 304 stars, we discard two, because their spectra were noisy and very sparse in time. The spectra are accessible from the ESO archives².

We now implement an extended sample with more data which were taken during 2011 to 2014 as part of the HARPS program extension. We use our B-index to determine any signs of activation periodicity in the time series. All of stars in our sample at least have 4 measurements and a total time span of observations covers at least 750 days. We divided the whole observation periods of each star to bins of 150 days then averaged all data points within each bin.

The fundamental stellar parameters ($vsini$, spectral type, T_{eff} , $\log g$, and [Fe/H]) were derived by Sousa et al. (2008) using the same HARPS spectra that we used here. Absolute magnitudes and luminosities derived from the Hipparcos catalogue. Table 1 lists the sample stars. The first three columns of table 1 show the star's name (HD name), the number of observations and their observation time span, respectively.

² The HARPS webpage: <http://www.eso.org/instruments/harps/>

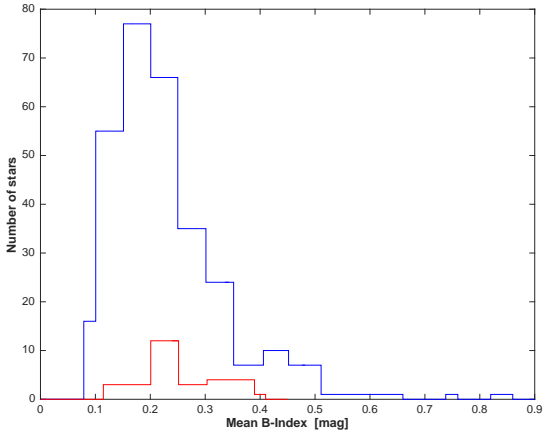


Figure 1. Distribution of the mean B-index values for 302 stars in the sample (blue). The same plot for 28 subgiants in the sample (red).

4 HARPS B-INDEX PROPERTIES

4.1 Distribution of the mean B-indices

Figure 1 shows distribution of mean B-index, calculated using equation 1, for 302 stars in the sample. The fourth and fifth columns of Table 1 shows the mean and standard deviation of B-index for all stars, respectively. The coolest star in the sample has an effective temperature of 4600 K which according to Bidaran, Mirtorabi & Azizi (2016) calibration is associated with a photospheric B-index of less than 0.05. Figure 1 clearly shows that all of the stars in the sample exhibit high level of TiO absorption in the photospheres which are too hot to sustain TiO molecules. Mirtorabi et al. (2003) have associated this TiO excess to cool spots which could be assumed as a tracer of activity, similar to the sun. The distribution displays a large peak around 0.2 and a smaller one in the tail between 0.4 and 0.5. Most of the stars have B-index between 0.15 - 0.3 with an average of 0.22. According to calibration this level of TiO is associated with cool regions with $T \sim 4000\text{ K}$ or $\sim 1200\text{ K}$ cooler than average effective temperature of the sample. This is another evidence to confirm this TiO is coming from stellar spots. At the tail of the distribution there is a smaller peak which represents a smaller sample of stars with relatively higher level of activity with spots as cool as 3800 K . The low level of the second peak with respect to the first one indicates that, as (Lovis et al. 2011) asserts, the sample mostly contains native solar-type stars with less active ones. The lower (red) distribution in the figure 1 shows a subsample of the stars which contain subgiants. Searching the SIMBAD we found 28 subgiants in the sample. The average value of B-index in subgiants are 0.23 which is higher than dwarf. This might be due to cooler atmosphere of these stars which are more prone to sustain TiO molecules than dwarfs.

4.2 Impact of metallicity on the mean B-index

Figure 2 shows the mean B-index values as a function of stellar metallicity for all stars in the sample. The metallicity of these stars have been calculated by Sousa et al. (2008) im-

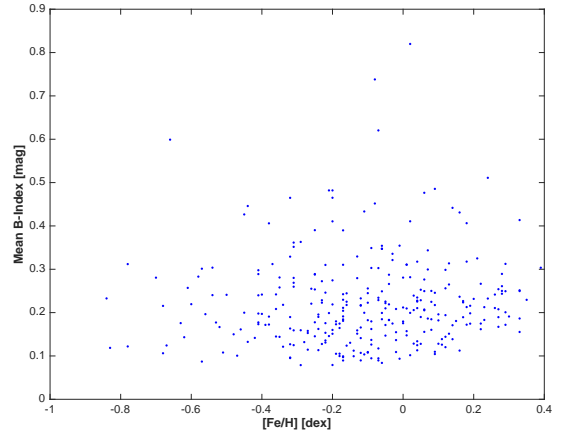


Figure 2. Mean B-index as a function of stellar metallicity.

plementing the same HARPS spectra that we used here. No evidence of correlation between mean B-index and $[Fe/H]$ can be recognized from figure 2. This result is consistent with previous findings that TiO absorption strength is independent of metallicity (Wing & White 1978). This is also in agreement with results of Lovis et al. (2011).

4.3 B-Index dispersion and noise

Figure 3 shows distribution of standard deviations (dispersion) of the B-index for 302 stars in the sample. Apart from large peak at 0.05 that might be produced by the observational noise, the distribution shows a smaller peak at about 0.3. Highly dispersed TiO absorption in long-term observation could be interpreted as periodic reappearance of cool, active regions in atmosphere of star. This small peak indicates that at least part of this sample might have experienced a period of stellar activity during last ten years.

To clarify that B-index has capability to resemble stellar activity we plot B-index dispersion versus mean B-index. Figure 4 shows that stars with higher B-index show more index variations. Higher B-index is an indication of existence of active regions like spots which regularly occurs when star is active. These stars are prone to have activity cycles and must exhibit higher value for B-index dispersion. B-index variability could also be caused by rotation of cool regions around the star which regularly resembles short period variation in B-index. We eliminate this type of variability by avoiding very low periods (less than two years).

5 METHOD AND ANALYSIS

Indices based on TiO absorption band have shown their potential to reveal active regions in surface of stars like λ Andromeda (Mirtorabi et al. 2003). The large data set in hand, provides us a unique opportunity to check this capability in a more reliable and statistically approved way. Our main goal is to search for significant long-term periodicities in the sample stars, according to their $TiO\lambda 567$ nm variation.

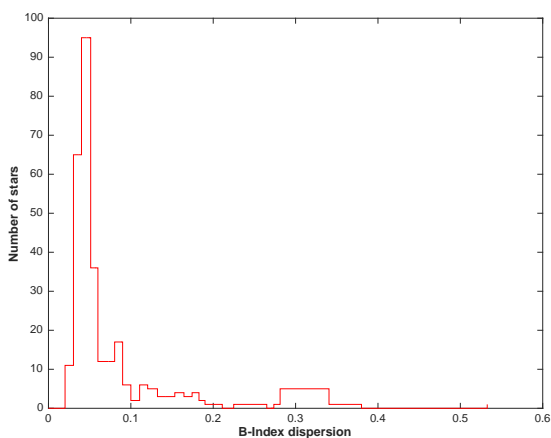


Figure 3. Distribution of B-index dispersions for all stars in the sample.

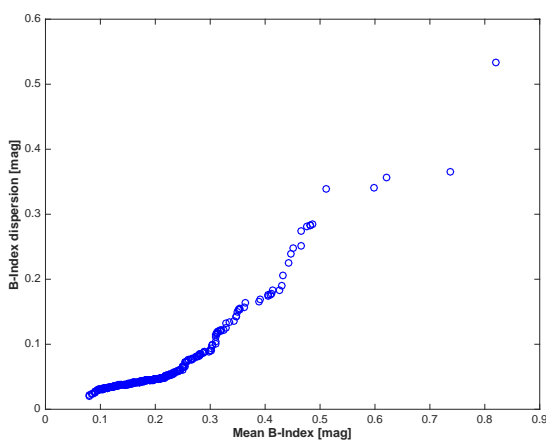


Figure 4. B-index dispersion as a function of mean B-index.

5.1 Periodicities

We derived the periodicity on the basis of results from calculations of power spectra of the time series. The most commonly used method of calculating the spectrum of non-uniformly spaced data is periodogram analysis (Lomb 1976; Scargle 1982). It is equivalent to least-squares fitting of sine and cosine waves, in form of $y = a \cos \omega t + b \sin \omega t$. The normalized periodogram analysis yields the best sinusoid that fits the unevenly sampled data, and the significance of the period is inferred from its false alarm probability (*FAP*) (Sturrock & Scargle 2010).

In order to search for activity cycles, we computed generalized Lomb-Scargle periodogram (*GLS*) for each star. The *GLS* is an extension to the Lomb-Scargle periodogram which takes into account the measurement of errors and also is more suitable for time series with none zero average. *GLS* tries to fit the equation $y = a \cos \omega t + b \sin \omega t + C$ to the time series and find the spectrum for frequencies (Zechmeister & Kurster 2009).

We consider a given periodogram peak, derived from *GLS* significant when it exceed the one present "false alarm

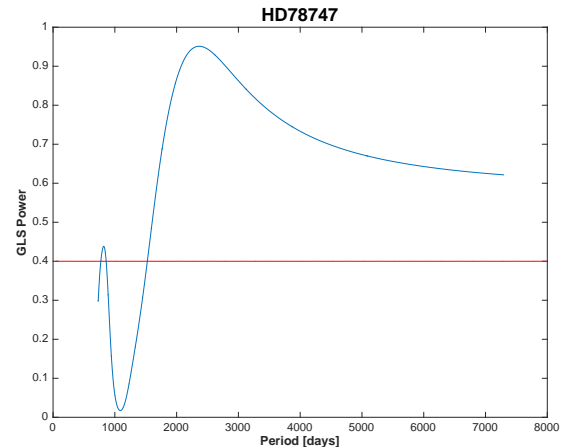


Figure 5. GLS periodogram of the B-index for HD78747, The red line denotes the 1% false-alarm probability.

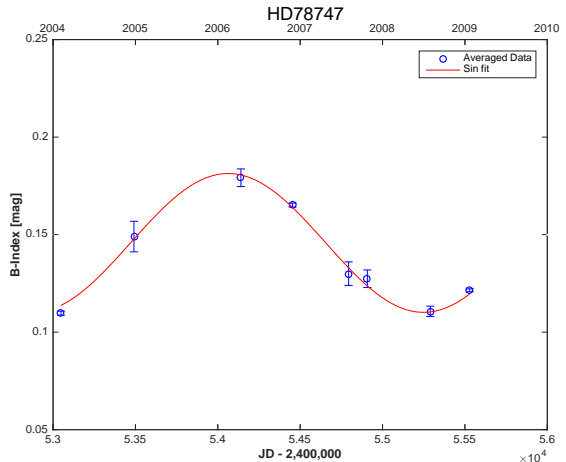


Figure 6. Time series of the B-index with the fitted activity cycle for HD78747.

probability" level (*FAP*), which means there is 99% confidence that the peak is real and could not be simulated by Gaussian noise. *FAP* levels are calculated by performing random permutations of the data with similar times of observations. To confirm that the period represented by the peak is appropriate, we rechecked the period by fitting a rescaled sin wave with that period to the data. Figure 5 and 6 show the periodogram and fitted sin wave for the star HD78747. Both figures indicates a significant activity cycle at a period of 2371 days.

To reduce the risk of inclusion of rotational variables from the final sample of active stars, we select a lower limit for the calculated peaks in periodograms. Peaks with period less than 2 years were discarded and we focused here on activity cycles in the 2 - 20 yr range. The 2 years time scale would be a relevant minimum for separating two variability regimes. It is more than 30 times larger than the rotational period of the sample and about five times smaller than activity period of the Sun. Main sequence stars with rotational periods higher than 2 years are rare and this minimum might appropriately disentangle any sign of rotational

variability from final results. A time scale of 20 years was selected as an upper limit for activity because typical time span of observations were limited to $\sim 10 - 11$ years.

Using Mont Carlo simulation we calculate confidence intervals for each measured period. A Gaussian distribution was used to generate different noise realization for each individual data points, with the same standard deviation taken from computed short-term scatter. By recomputing of *GLS* periodograms a confidence interval was calculated from distribution of derived periods.

5.2 Result

The results of the B-index analysis for determination of activity cycle are given in table 1 for all stars in the sample. 156 stars show significant activity cycle. The sixth and seventh columns of table 1 tabulates the activity period and the cycle semi-amplitude calculated from B-index. For those stars that have shown cycles in both indices we have also added their R'_{HK} period in the last column.

5.2.1 Activity cycles

Among 302 FGK stars, we find 156 stars with a detected cycle. There are 146 stars with no significant periodic variation. In the active subsample there are 153 stars with a cycle semi-amplitude larger than 0.01, where we assigned them as large-amplitude cycles. This is more than 51% of the sample. This is significantly greater than what Lovis et al. (2011) obtained by searching activity cycle in the variation of *CaII H&K* emission. No clear correlations between R'_{HK} index used by Lovis and B-index was found. 61% of Lovis active stars were also active in our B-index results.

5.2.2 Periods and amplitudes

Figure 7 shows the distributions of activity cycle periods. The histogram represents a maximum at 3000-4000 days and a smooth decrease for longer periods, unlike Lovis results that has steeper decrease. This might be due to that Lovis survey was not long enough to properly contain periods beyond ~ 4000 days. About 47% of the stars in the sample show an activity period similar to the Sun.

The distribution of activity cycle semi-amplitude is shown in figure 8. The sharp peak at ~ 0.03 belongs to those stars with semi-amplitude smaller than 0.01. They are mostly cycles that are not strong enough to result in a period with high confidence level or may be due to inactive stars or stars with very long activity cycle with no significant variation in the observation time span.

Figure 9 shows plot of activity cycle's semi-amplitude as a function of mean activity level (mean B-index). Although most of the stars with lower activity level ($0.1 \leq B\text{-index} \leq 0.25$) are concentrated in lower region with semi-amplitude less than 0.05, a few with higher B-index display a trend to have larger amplitude. The trend is disperse and not obvious. These are stars with activity period as short as they can illustrate a complete period in the course of whole observation like HD78747 shown in figure 6.

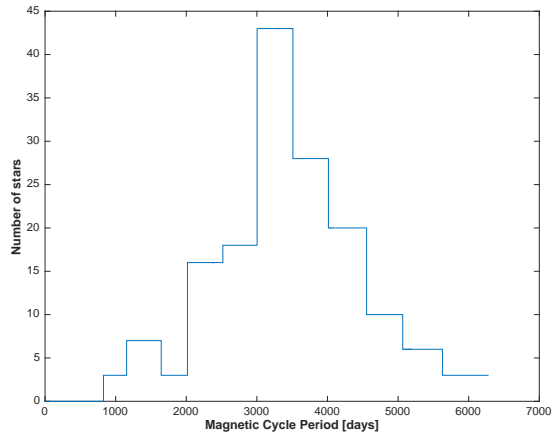


Figure 7. Distribution of activity cycle periods for 156 stars exhibiting long-term modulations in B-index.

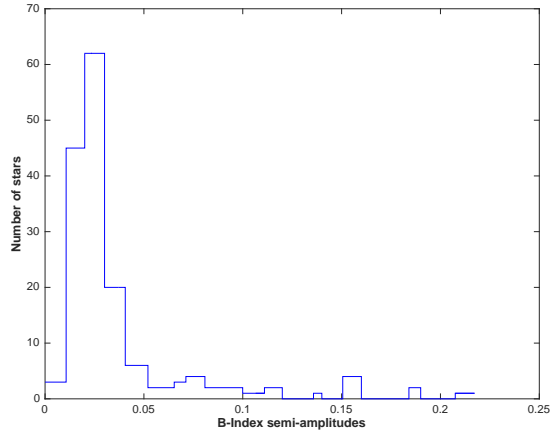


Figure 8. Distribution of activity cycle semi-amplitude for the 156 stars exhibiting long-term modulations in B-index.

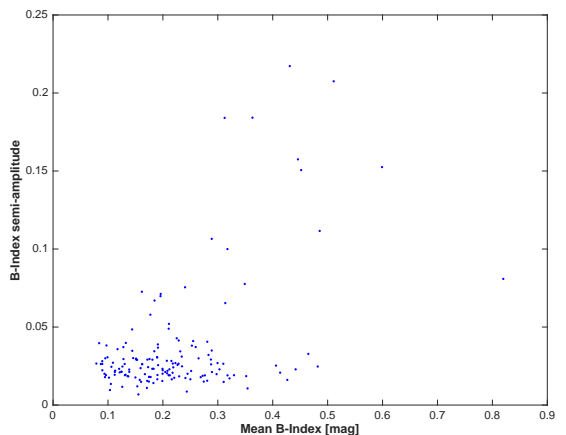


Figure 9. Activity cycle semi-amplitude as a function of mean B-index.

6 DISCUSSION AND CONCLUSION

The present survey has allowed us to measure activity cycles in a sample of solar-type stars by using molecular absorption bands. We are using a temperature sensitive index which measuring strength of an absorption band of the $\text{TiO}\lambda 567$ nm as a proxy to the activity cycle. This molecule is normally appear in cool and active regions of star surface.

In this work we have performed a similar study like Lovis et al. (2011) in a sample of old solar-type stars. The data sample was taken from high-precision spectrograph, HARPS, (Mayor et al. 2003). It spans 10 - 11 years of observation, compared to 7 - 8 years of the Lovis et al. (2011) survey. The longer time span allowed us to detect cycles with periods up to ~ 17 yr. Among all, 51.7 % of stars show a meaningful activity cycle. Since the B-index is high when the star is highly active. The lack of activity in some stars may be due to that they are in their quiet stage.

The distribution of activity cycle periods show a peak between 8-11 years, and smoothly decrease in both side of longer and shorter periods, compared to Lovis et al. (2011) who have calculated a sharper decrease towards longer periods. This sharp decrease may be due to insufficient number of stars with long observation time span to reveal a possible long-period cycles. Our results are roughly compatible with the results of Baliunas et al. (1995) (see their figure 3). In their studies a few of the stars are showing activity cycles with periods greater than 15 years. This confirms that our lower time duration than Baliunas et al. (1995) does not significantly affect the derived result for activity cycles.

No clear correlations between R'_{HK} index used by Lovis and B-index was found. We have four stars (HD 15337; HD 20794; HD125881; HD215152) with quiet B-index and significantly variable R'_{HK} . It seems hard to justify why two indices give different cycles. The sample of spectra we got from HARPS normally are sparse. The spectra are in groups of few tens taken in few days and groups are few months apart. Because few days are too short in our cycle investigation, we did average all the B-index inside a group. The error bars in the time series plots (figure 6) are calculated from relative dispersion of B-indices in a group. Appendix A shows that although the B-index varies significantly over the years which could be assumed as stellar activity but since averaged points are too sparse, a more continuous and evenly spread in time observation needed to find out whether these two indices are really correlated or not.

Apart from the lack of correlation between results from two indices, this work illustrates that molecular bands can also be used as a proxy to stellar activity and reveals the long period variation of stellar characteristics.

ACKNOWLEDGMENTS

This research is based on observations collected with the HARPS spectrograph on the 3.6-m telescope at *La Silla* Observatory, European Southern Observatory, Chile, Science Archive Facility. We thank the anonymous referee for the helpful comments and suggestions. M.T.M. is financially supported by the Alzahra university office of research and technology. FA is financially supported by the Payame Noor University.

REFERENCES

- Azizi F., Mirtorabi M. T., 2015, Ap&SS, 357, 96
- Baliunas S. L., Donahue R. A., Soon W. H., et al, 1995, ApJ, 438, 269
- Berdyugina S. V., Frutiger C., Solanki S. K., Livingston W., 2000, A&A, 364, 101
- Bidaran B., Mirtorabi M. T., & Azizi F., 2016, MNRAS, 457, 2043
- Boisse I., Moutou C., Vidal-Madjar A., et al., 2009, A&A, 495, 959
- Circunegui C., Diaz R. F., & Mauas P. J. D., 2007, A&A, 469, 309
- Diaz R. F., Circunegui C., & Mauas P. J. D., 2007, MNRAS, 378, 1007
- Gomes da Silva, Santos N. C., Bonfils X., Delfosse X., Forveille T., & Udry S., 2011, A&A, 534, 17
- Lomb N. R., 1976, Ap. Space Sci, 39, 447
- Lovis C., Dumusque X., Santos N. C., Bouchy F., Mayor M., Pepe F., Queloz D., Segransan D., Udry S., 2011, Arxiv e-prints, 1107.5325L
- Mayor M., Pepe F., Queloz D., Bouchy F., Rupprecht G., Lo Curto G., Avila G., Benz W., Bertaix J. L., Bonfils X., Dall Th., Dekker H., Delabre B., Eckert W., Fleury M., Gilliotte A., Gojak D., Lizone J. L., Longinotti A., Lovis C., Megevand D., Pasquini L., Reyes J., Sivan J. P., Sosnowska D., Soto R., Udry S., Van Kesteren A., Weber L., and Weilenmann U., 2003, The Messenger, 114, 20
- Mirtorabi M. T., Wasatonic R., Guinan E. F., 2003, AJ, 125, 3265
- Neff J. E., O’Neal D., Saar S. H., 1995, ApJ, 452, 879
- O’Neal D., Saar S. H., Neff J. E., 1996, ApJ, 463, 766
- O’Neal D., Neff J. E., Saar S. H., 1998, ApJ, 507, 919
- Ramsey L. W., Nations H. L., 1980, SAOSR, 389, 97
- Santos N. C., Mayor, M., Naef, D., et al, 2000, A&A, 361, 265
- Saar S. H., Huovelin J., Osten R. A., & Shcherbakov, A. G., 1997, A&A, 326, 741
- Scargle J. D., 1982, ApJ, 835, 853
- Sousa S. G., Santos N. C., Mayor M., et al., 2008, A&A, 487, 373
- Sturrock P. A., Scargle J. D., 2010, ApJ, 18, 527
- Wallace L., Meyer M. R., Hinkle K., Edwards S., 2000, ApJ, 535, 325
- Wilson O. C., 1968, ApJ, 153, 221
- Wilson O. C., 1978, ApJ, 226, 379
- Wing R. F., 1992, JAVSO, 21, 42
- Wing R. F., White, N. M., 1978, IAUS, 80, 45
- Zechmeister M., Kurster M., 2009, A&A, 496, 577

Table 1: The Results

<i>Star HD name</i>	<i>No. Obs.</i>	<i>Observed time(days)</i>	<i>B – Index</i>		<i>Period (days)</i>	<i>Semi– amplitude</i>	<i>Period R'_{HK} (days)</i>
55	60	3647	0.599	0.249	2730^{+208}_{-208}	0.152	
361	58	3685	0.0897	0.0436	1729^{+10}_{-12}	0.0223	
967	64	2556	0.216	0.100	2624^{+382}_{-386}	0.0283	
1320	20	3230	0.115	0.0455			
1388	59	3398	0.0936	0.0372	2032^{+1237}_{-1237}	0.0201	
1461	190	3688	0.174	0.0821	2317^{+295}_{-295}	0.0151	3754^{+807}_{-565}
1581	118	3242	0.175	0.103			
3569	121	3677	0.0951	0.0366	3897^{+1022}_{-1022}	0.0300	
3823	69	2226	0.132	0.0422			
4307	93	3676	0.223	0.177	2948^{+2089}_{-2091}	0.159	
4308	182	3358	0.218	0.0336	5066^{+448}_{-500}	0.0266	
4915	44	1770	0.199	0.118	2140^{+850}_{-750}	0.0154	1863^{+1951}_{-211}
6348	21	3328	0.196	0.0291			
6673	20	1142	0.255	0.122			
6735	31	3654	0.0840	0.0495	2927^{+120}_{-120}	0.0397	
7134	22	3663	0.0789	0.0439	4125^{+159}_{-136}	0.0266	
7199	116	3639	0.289	0.0490	5873^{+2}_{-6}	0.0212	2760^{+416}_{-319}
7449	108	3346	0.104	0.0347	3060^{+394}_{-383}	0.00963	
8638	50	3293	0.191	0.0830	2399^{+336}_{-362}	0.0389	
8828	55	3704	0.218	0.0666	$1365^{+0.3}_{-4}$	0.0207	2163^{+300}_{-234}
9246	49	3328	0.177	0.0766	3296^{+2324}_{-2324}	0.0579	2747^{+540}_{-387}
9782	30	2217	0.104	0.0311			
9796	22	2855	0.253	0.142			
10002	30	3331	0.189	0.0727	2487^{+1268}_{-1238}	0.0307	
10180	192	3387	0.160	0.0384	4312^{+646}_{-587}	0.0149	2737^{+414}_{-318}
10700	192	2560	0.167	0.0481			
11226	44	1766	0.134	0.0399			
11505	24	3325	0.131	0.0423	4033^{+1583}_{-1583}	0.0191	
11964	159	3677	0.250	0.0534	5403^{+414}_{-475}	0.0165	
12345	43	3574	0.146	0.0557	4115^{+842}_{-867}	0.0301	
12387	95	3246	0.196	0.0844	2357^{+87}_{-83}	0.0855	
12617	94	3246	0.196	0.0847	2658^{+13}_{-4}	0.0712	
13060	92	3689	0.282	0.0443			
13724	36	3621	0.183	0.0451			
13808	190	3672	0.274	0.0433	5897^{+1130}_{-832}	0.0150	3715^{+807}_{-562}
14374	19	2089	0.219	0.0579			
14747	20	2379	0.172	0.0452	2739^{+243}_{-246}	0.0291	
15337	46	3643	0.250	0.0381			
16297	60	3651	0.354	0.0845			
16417	184	3729	0.151	0.0411	6282^{+4369}_{-4419}	0.0292	
16714	185	3729	0.151	0.0411	6003^{+867}_{-936}	0.0297	
17970	35	3690	0.200	0.0596			
19034	30	3660	0.150	0.0450	3494^{+102}_{-83}	0.0177	
19467	51	3774	0.112	0.0467	3736^{+940}_{-940}	0.0194	
20003	184	3695	0.210	0.0319	4854^{+110}_{-110}	0.0191	3149^{+562}_{-414}
20407	65	3693	0.446	0.366	3364^{+222}_{-222}	0.212	
20619	36	2138	0.153	0.0317	2043^{+9}_{-4}	0.0120	1687^{+184}_{-151}
20781	167	3734	0.200	0.0527	4136^{+32}_{-11}	0.0223	$8000^{+\infty}_{-4249}$
20782	165	3734	0.199	0.0529	4033^{+30}_{-10}	0.0232	1150^{+65}_{-58}
20794	168	763	0.242	0.126			
20807	150	3692	0.228	0.183	2413^{+11}_{-3}	0.0265	1133^{+1090}_{-65}
21019	47	3752	0.173	0.0342	2865^{+153}_{-153}	0.0161	
21209	44	3259	0.426	0.122			

Continued on next page

Table 1 – continued from previous page

<i>Star</i> <i>HD name</i>	<i>No.</i>	<i>Observed</i> <i>time(days)</i>	<i>B – Index</i>	<i>Period</i> <i>(days)</i>	<i>Semi-</i> <i>amplitude</i>	<i>Period</i> <i>R'HK (days)</i>
21693	190	3412	0.212	0.0325	3842^{+2214}_{-2214}	0.0229
21938	22	3341	0.101	0.0368		2483^{+322}_{-256}
22879	100	3778	0.119	0.0757		
23249	177	3777	0.314	0.120	3974^{+30}_{-9}	0.0653
23356	33	2228	0.310	0.0308		
23456	28	3429	0.0963	0.0373	4033^{+258}_{-268}	0.0192
24331	11	2700	0.280	0.0512		
24892	27	3428	0.163	0.0322		
25673	23	3427	0.241	0.0357	3179^{+431}_{-413}	0.0173
26965	136	3368	0.269	0.177	3282^{+20}_{-7}	0.0179
27063	45	1576	0.190	0.0387	1352^{+160}_{-155}	0.0165
28471	30	3378	0.210	0.0861		3352^{+805}_{-543}
28701	23	3223	0.190	0.0403		1316^{+153}_{-124}
28821	26	3665	0.141	0.0406		
30278	29	1514	0.242	0.0450		
30306	22	2905	0.224	0.0571		
31527	27	3612	0.211	0.0931	2658^{+500}_{-493}	0.0433
31822	192	3612	0.105	0.0376		
32724	33	3673	0.0973	0.0455	3465^{+15}_{-15}	0.0382
33725	25	3671	0.184	0.0443	3759^{+545}_{-567}	0.0397
34449	61	3791	0.0946	0.0362		
34688	22	3383	0.219	0.0418	3974^{+29}_{-9}	0.0242
35854	42	3816	0.279	0.0410		2026^{+208}_{-172}
36003	196	3411	0.482	0.0303		
36108	25	3467	0.0720	0.0411	3480^{+872}_{-872}	0.0247
36379	95	3810	0.0896	0.0422	4312^{+36}_{-10}	0.0281
37986	20	3340	0.211	0.0471	3603^{+41}_{-41}	0.0489
38277	20	3386	0.117	0.0430	2582^{+573}_{-536}	0.0358
38858	176	3763	0.136	0.0435	4580^{+38}_{-14}	0.0186
38973	30	3345	0.128	0.0476	3702^{+372}_{-372}	0.0353
39194	178	2915	0.257	0.135		3406^{+570}_{-428}
40105	52	3675	0.276	0.0433	3350^{+356}_{-360}	0.0190
40307	170	3010	0.362	0.0325		
40397	40	3824	0.159	0.0326		
44120	43	3707	0.120	0.0390	3130^{+404}_{-387}	0.0232
44420	22	3375	0.172	0.0460		
44447	60	3676	0.246	0.190		
44573	73		0.620	0.252		
44594	40	3290	0.181	0.0417	2495^{+28}_{-12}	0.0232
45184	166	3772	0.125	0.0514	3753^{+1233}_{-1173}	0.0213
45289	92	3771	0.109	0.0459	3788^{+195}_{-173}	0.0271
45364	85	3636	0.191	0.0579	4825^{+44}_{-13}	0.0256
47186	135	3761	0.213	0.116	4740^{+408}_{-369}	0.0191
48611	17	1225	0.242	0.0589		
50590	20	3074	0.310	0.0482	2959^{+1075}_{-1084}	0.0264
50806	74	1819	0.206	0.0410		
51608	172	3715	0.229	0.116	3480^{+708}_{-727}	0.0414
55693	38	3434	0.312	0.282	3106^{+43}_{-18}	0.184
52919	4	1021	0.390	0.0286		2403^{+266}_{-218}
59468	190	3756	0.239	0.0440		
59711	47	3771	0.107	0.083		
63765	53	2303	0.225	0.0578	2284^{+859}_{-864}	0.0172
65277	27	3716	0.352	0.0360	3652^{+802}_{-802}	0.0185
65562	46	3629	0.223	0.0579	3378^{+137}_{-124}	0.0269
65907	61	3466	0.125	0.0404	4244^{+301}_{-316}	0.0188
						$8000^{+\infty}_{-2216}$

Continued on next page

Table 1 – continued from previous page

<i>Star</i> <i>HD name</i>	<i>No.</i> <i>Obs.</i>	<i>Observed</i> <i>time (days)</i>	<i>B – Index</i> <i>mean</i>	<i>σ</i>	<i>Period</i> <i>(days)</i>	<i>Semi-</i> <i>amplitude</i>	<i>Period</i> <i>R'HK (days)</i>
66221	50	3629	0.227	0.0602	3771^{+119}_{-100}	0.0258	
67458	48	3463	0.124	0.0534			
68607	50	1210	0.299	0.0462	899^{+78}_{-80}	0.0269	$863^{+\infty}_{-130}$
68978	126	3759	0.113	0.0381	3571^{+23}_{-8}	0.0221	1021^{+58}_{-310}
69655	51	3465	0.165	0.239			
69830	193	3670	0.249	0.0731			
70889	20	1580	0.139	0.0282	1232^{+446}_{-439}	0.0213	
71334	42	3724	0.126	0.0450	3619^{+56}_{-43}	0.0247	
71479	73	3387	0.511	0.341	2002^{+8}_{-4}	0.0475	1525^{+1993}_{-114}
71835	78	3731	0.183	0.0425	3685^{+17}_{-17}	0.0232	3222^{+565}_{-418}
72579	39	2975	0.232	0.117	2843^{+75}_{-59}	0.0214	
72673	162	3001	0.240	0.0437			
72769	32	3385	0.191	0.0664	4942^{+1145}_{-1167}	0.0368	
73121	136	3420	0.110	0.0525			
73524	159	3420	0.112	0.0541	3217^{+57}_{-31}	0.0212	2801^{+984}_{-322}
74014	25	3069	0.175	0.0419	4685^{+428}_{-452}	0.0181	
78429	68	3790	0.246	0.182			
78558	24	3810	0.133	0.0660	3350^{+107}_{-107}	0.0398	
78612	22	3071	0.113	0.0515			
78747	53	2554	0.124	0.0344	2371^{+147}_{-147}	0.0213	2389^{+316}_{-250}
81639	24	3109	0.181	0.0481	2767^{+213}_{-224}	0.0291	
82342	52	3720	0.240	0.136	3256^{+80}_{-80}	0.0755	3434^{+571}_{-428}
82516	71	3719	0.311	0.0466	2703^{+634}_{-612}	0.0148	$6065^{+\infty}_{-4074}$
83529	28	3685	0.176	0.165	2855^{+1463}_{-1464}	0.0295	
85390	8	3682	0.234	0.0879	2835^{+163}_{-140}	0.0311	2476^{+322}_{-255}
85512	105	3467	0.465	0.0482	3130^{+248}_{-248}	0.0328	3793^{+806}_{-566}
86065	28	3110	0.289	0.0473			
86140	43	3098	0.347	0.0995	3003^{+17}_{-5}	0.0350	2798^{+418}_{-1427}
86171	121	1960	0.390	0.0571			
88084	24	3071	0.109	0.0447			
88218	61	3813	0.0994	0.0355			
88742	49	3435	0.155	0.0325			
89454	59	2218	0.299	0.225			
90156	152	3434	0.162	0.0725	4013^{+69}_{-107}	0.0263	1279^{+81}_{-72}
90711	27	3339	0.233	0.0445			
90812	29	3339	0.208	0.0465	3510^{+18}_{-12}	0.0219	$8000^{+\infty}_{-2419}$
92588	120	2343	0.235	0.0754	2017^{+7}_{-3}	0.0248	
92719	67		0.108	0.0451			
93083	106	3434	0.486	0.281	3378^{+114}_{-137}	0.112	3453^{+806}_{-550}
93385	177	3788	0.102	0.0441	3619^{+842}_{-828}	0.0176	
94151	55	3385	0.318	0.166	4538^{+26}_{-9}	0.999	3792^{+806}_{-566}
95456	166	3748	0.431	0.356	3510^{+25}_{-5}	0.199	
95521	24	3383	0.130	0.0410	4554^{+1478}_{-1487}	0.0232	
96423	69	3722	0.128	0.0526	3243^{+21}_{-3}	0.0295	
96700	167	3696	0.105	0.0458	3083^{+1065}_{-1020}	0.0135	$830^{+\infty}_{-27}$
97037	87	3693	0.0897	0.0331	4768^{+2451}_{-2451}	0.0263	
97343	77	4160	0.185	0.111	5403^{+55}_{-18}	0.0670	
97998	25	3384	0.142	0.0518			
98281	66	3687	0.221	0.0381	1401^{+9}_{-4}	0.0175	2861^{+1354}_{-396}
100508	32	2284	0.304	0.0422			
101930	103	3436	0.265	0.0654	3230^{+381}_{-349}	0.0299	$8000^{+\infty}_{-2453}$
102117	119	3787	0.261	0.0637			
102438	87	3790	0.159	0.0403	4053^{+32}_{-9}	0.0237	
104006	91	4128	0.122	0.0992	4289^{+532}_{-564}	0.0890	

Continued on next page

Table 1 – continued from previous page

<i>Star</i> <i>HD name</i>	<i>No.</i> <i>Obs.</i>	<i>Observed</i> <i>time(days)</i>	<i>B – Index</i> <i>mean</i>	<i>Period</i> <i>(days)</i>	<i>Semi-</i> <i>amplitude</i>	<i>Period</i> <i>R'HK (days)</i>
104067	88	2271	0.347	0.0413		
104263	32	2245	0.199	0.0600	2123 ⁺⁴⁹⁵ ₋₄₇₈	0.0201
104982	47	3043	0.173	0.0659	2487 ⁺⁸⁹² ₋₈₅₁	0.0243
105837	26	3049	0.108	0.0902		
106116	109	3675	0.171	0.0401	3269 ⁺¹⁸ ₋₈	0.0110
106275	27	3010	0.303	0.0587	2317 ⁺³⁶⁸ ₋₃₆₈	0.0229
108309	49	3333	0.144	0.0478	5368 ⁺¹⁴¹ ₋₅₉	0.0347
109200	137	2966	0.260	0.0373		
109409	63	3333	0.155	0.0444	3142 ⁺⁶⁰⁰ ₋₅₈₅	0.00680
110619	36	3273	0.289	0.274	3243 ⁺¹³⁷ ₋₁₃₇	0.0474
111031	40	3337	0.167	0.0351	3014 ⁺¹⁷ ₋₅	0.0198
112540	12	3275	0.230	0.0489		
114613	195	3560	0.216	0.0529		
114747	39	1473	0.325	0.0361		
114853	62	3783	0.128	0.0462		
115585	33	3015	0.230	0.0529		
115617	164	2918	0.137	0.0382		
115674	39	2252	0.204	0.0271	3378 ⁺¹³¹⁸ ₋₁₃₂₁	0.0212
116920	14	2305	0.272	0.0402	2063 ⁺¹⁹⁵ ₋₁₉₅	0.0187
117105	46	3337	0.363	0.339	3060 ⁺¹²⁴ ₋₁₃₆	0.209
117207	63	3779	0.162	0.0730		
119638	27	3324	0.0945	0.0404	2992 ⁺¹²³³ ₋₁₂₃₃	0.0297
119782	19	2636	0.303	0.0369		
122862	50	3328	0.166	0.0520		
123265	35	4127	0.198	0.0749		
124292	31	3037	0.151	0.0383		
124364	18	3031	0.153	0.0417	3897 ⁺¹⁶⁷⁶ ₋₁₆₇₆	0.0289
125072	44	3653	0.406	0.0460		
125184	151	3749	0.189	0.0444	4033 ⁺³²⁵ ₋₃₂₅	0.0305
125455	132	3639	0.0997	0.0898		
125881	196	3603	0.476	0.282		
129642	64	1510	0.354	0.0283	828 ⁺³⁴ ₋₃₃	0.0107
126525	104	3675	0.182	0.0780		
128674	22	3028	0.172	0.0385		
130930	21	2882	0.311	0.0413		
130992	23	3266	0.329	0.0492	1922 ⁺⁷⁰ ₋₇₀	0.0191
132648	40	3002	0.312	0.153		
134060	172	3748	0.139	0.0312	3230 ⁺⁷¹² ₋₇₁₂	0.0228
134606	174	3602	0.208	0.0314	6282 ⁺⁴⁷⁸ ₋₅₀₇	0.0203
134664	33	1067	0.182	0.0319		
134985	23	3030	0.220	0.0374		
136352	177	3495	0.121	0.0389	3435 ⁺⁷⁷ ₋₇₁	0.0209
136713	43	2203	0.344	0.0375		
136894	50	2044	0.256	0.0806		
137303	44	2044	0.258	0.0803		
137388	91	2942	0.318	0.0458	3974 ⁺³¹²⁰ ₋₃₁₂₀	0.0190
138549	23	2942	0.176	0.0461	3105 ⁺³³ ₋₄₀	0.0180
140901	47	1429	0.217	0.0546		
142709	81	3329	0.281	0.132		
143114	21	3113	0.177	0.0583		
144411	16	2481	0.329	0.0433		
144585	168	2904	0.186	0.0759		
144628	47	2105	0.298	0.0334	2697 ⁺⁷²⁹ ₋₇₃₆	0.0193
145598	44	2107	0.312	0.533		
145666	26	3970	0.266	0.0822		
145809	34	2906	0.145	0.0605		

Continued on next page

Table 1 – continued from previous page

<i>Star</i> <i>HD name</i>	<i>No.</i> <i>Obs.</i>	<i>Observed</i> <i>time (days)</i>	<i>B – Index</i> <i>mean</i>	<i>Period</i> <i>(days)</i>	<i>Semi-</i> <i>amplitude</i>	<i>Period</i> <i>R'_{HK}</i> <i>(days)</i>
146233	200	1147	0.228	0.0232		
147512	54	1734	0.452	0.284	1722^{+6}_{-2}	0.201
148303	72	3215	0.321	0.0512	3540^{+602}_{-620}	0.0171
150433	91	3204	0.145	0.0419		
151504	21	2261	0.205	0.0201		
154088	187	2701	0.244	0.0445	4659^{+80}_{-56}	0.00864
154363	126	2999	0.143	0.0388		
154577	109	3390	0.281	0.0307	3824^{+139}_{-119}	0.0156
157338	200	2936	0.820	0.177		
157172	186	2891	0.126	0.0855	1354^{+36}_{-40}	0.0117
157347	132	3566	0.738	0.153	4013^{+307}_{-287}	0.0809
157830	67	3024	0.178	0.0415	3435^{+229}_{-252}	0.0180
161612	56	4021	0.237	0.174		
161098	116	2696	0.158	0.0376	3480^{+86}_{-53}	0.0161
162236	43	3496	0.233	0.0727		
162396	83	3351	0.144	0.0643	3954^{+1551}_{-1562}	0.0435
165920	55	3660	0.201	0.0886		
166724	71	3347	0.349	0.142	2641^{+31}_{-31}	0.0981
168871	125	3079	0.137	0.0352	3014^{+1314}_{-1314}	0.0184
170493	31	3237	0.442	0.0582	4335^{+572}_{-589}	0.0229
171665	20	2512	0.171	0.0366	3060^{+929}_{-934}	0.0155
171990	73	1797	0.207	0.0528	1382^{+223}_{-226}	0.0284
172513	44	1081	0.222	0.0331		
174545	35	3081	0.266	0.0610		
176986	170	3867	0.281	0.0887	2845^{+758}_{-758}	0.0406
177409	34	3221	0.183	0.0251	3897^{+2419}_{-2419}	0.0141
177565	74	3641	0.185	0.0452	6003^{+2298}_{-2357}	0.111
177758	165	3867	0.283	0.0867	3003^{+68}_{-68}	0.0321
180409	22	3257	0.0992	0.0456	3243^{+1483}_{-1485}	0.0306
181433	190	3877	0.413	0.0516	4094^{+195}_{-197}	0.0208
183658	54	3571	0.129	0.0540		
183783	26	3678	0.411	0.0893		
185615	19	2947	0.225	0.0588		
187456	21	3639	0.411	0.0346		
188559	33	796	0.433	0.0340		
188748	20	2133	0.216	0.0270	2048^{+617}_{-622}	0.0173
189567	198	3640	0.190	0.0451	5789^{+61}_{-22}	0.0193
189625	57	1758	0.172	0.0325		
190248	193	2911	0.251	0.0440	3935^{+19}_{-19}	0.0218
190954	24	3062	0.198	0.0524		
192031	22	3376	0.233	0.206		
192310	196	3287	0.287	0.154	3392^{+1781}_{-1786}	0.0292
193193	52	2889	0.147	0.0420		3792^{+806}_{-566}
195564	63	3869	0.156	0.0360		
196761	68	3869	0.159	0.0598		
197210	19	2831	0.175	0.0492		
197823	23	1056	0.256	0.0433		
199288	198	3963	0.176	0.0215		
199960	150	3294	0.250	0.169		
203384	29	2834	0.242	0.0900		
203432	73	1405	0.249	0.0325		
203850	22	3281	0.106	0.0315	3435^{+256}_{-256}	0.0279
204313	158	3277	0.213	0.122		
204385	21	2890	0.186	0.0402		
204941	176	3462	0.180	0.0773		

Continued on next page

Table 1 – continued from previous page

<i>Star</i> <i>HD name</i>	<i>No.</i> <i>Obs.</i>	<i>Observed</i> <i>time(days)</i>	<i>B – Index</i> <i>mean</i>	<i>σ</i>	<i>Period</i> <i>(days)</i>	<i>Semi-</i> <i>amplitude</i>	<i>Period</i> <i>R'HK (days)</i>
205536	60	3260	0.226	0.0432			
207129	186	1402	0.179	0.0243			
207700	60	3260	0.226	0.0432			
209100	198	956	0.465	0.119			
209742	26	3610	0.244	0.0368			
210752	27	3657	0.0871	0.0423	5628^{+331}_{-331}	0.0263	
210918	79	3889	0.180	0.0551			
211038	185	3887	0.288	0.0448	4554^{+468}_{-505}	0.0261	
212708	53	3693	0.254	0.0430			
213628	29	4172	0.147	0.0402			
213941	29	2218	0.161	0.0459			
215152	193	3630	0.301	0.0483			
215456	196	3892	0.162	0.0478	4713^{+42}_{-13}	0.0261	
219249	21	2901	0.197	0.0654			
220256	26	3680	0.245	0.0306	3480^{+792}_{-748}	0.0201	
220507	89	3601	0.157	0.0465			
221356	34	4221	0.0791	0.0369			
221420	66	3684	0.250	0.0308			
222237	37	3690	0.406	0.0360	4244^{+191}_{-191}	0.0253	2168^{+2049}_{-424}
222422	8	2522	0.217	0.0989			
222595	33	1687	0.210	0.0366			
222669	62	3656	0.229	0.0447			
223121	26	2252	0.253	0.0536	4136^{+2466}_{-2466}	0.0381	
223171	180	3893	0.194	0.0337			
224619	23	3280	0.160	0.0485			
224789	35	2833	0.336	0.0482			
hip22059	36	2584	0.127	0.150			
hip26542	5	1078	0.304	0.157			

APPENDIX A: TYPICAL EXAMPLES OF GLS PERIODOGRAM AND TIME SERIES FOR STARS WITH A SIGNIFICANT ACTIVITY CYCLE.

Here we present typical periodogram and time series for those stars that exhibit significant activity cycle. Column one shows the periodogram. The red horizontal line in the periodogram plot represents FAP level. Column two shows the time series for that star which fitted with a sinusoidal curve with period that maximize the periodogram. Column three and four is the same as one and two.

